Materials Science & Engineering C 89 (2018) 336–345

Contents lists available at ScienceDirect

Materials Science & Engineering C

journal homepage: www.elsevier.com/locate/msec

Silk fibroin/nanohydroxyapatite hydrogels for promoted bioactivity and osteoblastic proliferation and differentiation of human bone marrow stromal cells

Marta Ribeiro[a,b,c,*], Maria H. Fernandes[d,e], Marisa M. Beppu[f], Fernando J. Monteiro[a,b,c], Maria P. Ferraz[g]

[a] i3S - Instituto de Investigação e Inovação em Saúde, Universidade do Porto, Porto 4200-135, Portugal
[b] INEB - Instituto de Engenharia Biomédica, Universidade do Porto, Porto 4150-180, Portugal
[c] FEUP - Faculdade de Engenharia da Universidade do Porto, Departamento de Engenharia Metalúrgica e Materiais, Porto 4200-465, Portugal
[d] Laboratory for Bone Metabolism and Regeneration, Faculdade de Medicina Dentária, Universidade do Porto, Porto 4200-393, Portugal
[e] REQUIMTE/LAQV – U. Porto, Porto, Portugal
[f] School of Chemical Engineering, University of Campinas, Campinas, SP 13083-852, Brazil
[g] FP-ENAS/CEBIMED - University Fernando Pessoa Energy, Environment and Health Research Unit/Biomedical Research Center, Porto 4249-004, Portugal

ARTICLE INFO

Keywords:
Silk fibroin
Nanohydroxyapatite
Bioactivity
Osteoblast differentiation
Bone regeneration

ABSTRACT

Silk fibroin (SF) is a natural, biocompatible, and biodegradable polymer having a great potential for the successful regeneration of damaged bone tissue. In the present work, nanohydroxyapatite (nanoHA) was incorporated into SF polymer to form a bioactive composite hydrogel for applications as bone implants. The degradation and bioactive properties of SF/nanoHA composite hydrogels were evaluated. Additionally, biological investigations of human bone marrow stromal cells (hBMSCs) viability, proliferation and differentiation to the osteoblastic phenotype were conducted. The incorporation of nanoHA in SF polymer matrices improved the bioactivity of the hydrogels. The biological results highlighted that the SF/nanoHA composite hydrogels are suitable for hBMSCs attachment and proliferation, while a test for alkaline phosphatase (ALP) and bone morphogenetic protein 2 (BMP-2) expression suggested osteoblast differentiation. Additionally, a cell staining method for ALP allowed to observe cell infiltration with active production of ALP by the infiltrated cells, paving the way to use the proposed composite hydrogel for bone tissue regeneration.

1. Introduction

Scaffolds and cells are essential components in bone regenerative approaches. These scaffolds focus on developing biologically-based substitutes with similar structure and functionality to the extracellular matrix (ECM) in order to assist cell adhesion and proliferation. Biological scaffolds should gradually degrade to support the cell ingrowth and bone formation through the regeneration process, as well as to avoid the risk of complications that may be associated with the long-term presence of a foreign material [1–4]. Hydrogels have attracted extensive interest because of their advantageous properties similar to those of the native ECM, such as biocompatibility and the ability to absorb high amounts of water or biological fluids without dissolving, thus maintaining their three-dimensional (3D) structure and function. Their high permeability allows the exchange of oxygen, nutrients, and soluble metabolites [5–7].

Silk fibroin (SF) is a protein polymer derived from the cocoons of *Bombyx mori* which possesses adequate properties for bone tissue engineering scaffolds, such as biocompatibility, biodegradability, high permeability to oxygen and water vapor, versatile processing, and adjustable mechanical and biochemical properties [8–11].

SF-based composite hydrogels incorporating relevant molecules of the extracellular matrix such as SF/hyaluronic acid [12] and SF/collagen [13] have been reported to present enhanced physicochemical and biological properties for tissue engineering applications. In a different approach, the incorporation of a bioactive ceramic in the hydrogel matrix is expected to improve the osteogenic potential of the resulting composite. The presence of the bioactive ceramic inside a polymeric matrix would mimic the inorganic phase of the extracellular matrix favoring bone cell behavior and the interaction with the surrounding bone tissue [14,15]. In a previous study, we described the preparation of novel SF-hydrogels incorporating different percentages

* Corresponding author.
E-mail address: ribeiro_marta88@hotmail.com (M. Ribeiro).

https://doi.org/10.1016/j.msec.2018.04.034
Received 18 August 2017; Received in revised form 20 February 2018; Accepted 15 April 2018
Available online 16 April 2018
0928-4931/ © 2018 Elsevier B.V. All rights reserved.

of nanophased hydroxyapatite (0, 10, 15, 20 and 30 wt%) by using a new and innovative method, in which ethanol was used as gelling agent [8]. However, when the nanoHA content was higher than 15 wt%, nanoHA aggregation occurred. The SF hydrogel incorporating 15 wt% of nanoHA yielded a composite with improved mechanical properties [8] together with a higher amount of uniformly dispersed particles throughout the matrix, in combination with interconnected micro- and macroporosity suitable for new bone formation. Moreover, in the previous study, non-frozen and frozen hydrogels were evaluated in order to assess differences in the materials properties [8]. The main difference observed was the higher pore sizes for frozen materials (44.4 ± 38.2 μm: min 1.6 μm–max 255.3 μm) compared to non-frozen materials (19.1 ± 18.1 μm: min 1.4 μm–max 104.8 μm). Additionally, preliminary biological data performed with MG63 cells showed promising results regarding osteoblastic cell response [8].

Consequently, the main goal of the current work was to exploit the suitability of the SF/15% wt% nanoHA hydrogel for bone regenerative strategies. For that, the SF/nanoHA hydrogel was prepared as described previously [8] and evaluated for enzymatic degradation, bioactivity and ability to promote the proliferation and osteoblastic differentiation of human bone marrow stromal cells.

2. Materials and methods

2.1. Preparation of silk fibroin solution

Cocoons of *Bombyx mori* silkworm (supplied by Bratac, São Paulo, Brazil) were degummed in 1 g/L Na_2CO_3 solution at 85 °C for 1 h 30 min, with Na_2CO_3 being changed every 30 min to remove the sericin of the cocoons and obtain pure SF fibers. Then, SF fibers were dried and dissolved in a ternary solvent of $CaCl_2$:CH_3CH_2OH:H_2O, in a molar ratio of 1:2:8, at 85 °C until total dissolution, to a SF salt solution of 10% (w/v). The SF salt solution was then dialyzed (cellulose membrane, Viscofan 22 EU – 20 USA) against distilled water for 3 days, at 8 °C, with water being changed every 24 h. The final concentration of the SF aqueous solution was 4% (w/v), which was determined by weighing the remaining solid after drying.

2.2. Preparation of silk fibroin/nanoHA hydrogels

SF/nanoHA hydrogels were prepared according to our previously established method [8]. Briefly, the dry power of nanoHA aggregates (Fluidinova S.A., Maia, Portugal) was first mixed with 70% ethanol and then slowly mixed with the SF aqueous solution at 37 °C. SF and nanoHA were mixed at ratios of SF/nanoHA 100/0 and 85/15 wt%. The hydrogel containing 15% of nanoHA was called SF/nanoHA15. Part of these hydrogels was frozen at −20 °C for 24 h, through one freeze-thaw cycle, to evaluate differences in the properties of non-frozen and frozen hydrogels. The frozen hydrogels were identified with the letter F.

2.3. In vitro enzymatic degradation

In vitro enzymatic degradation of the hydrogels was measured *versus* time, by incubating the gels in protease XIV solution (*Streptomyces griseus*, Sigma) and monitoring the hydrogel mass. Hydrogels sections with 7 mm diameter and 5 mm thickness were carefully transferred to 48-well plates and soaked in phosphate-buffered saline solution (PBS, pH 7.4) overnight to reach swelling equilibrium. The gels were removed from PBS, excess liquid was blotted from the surface with filter paper, and the gel masses were determined. The gels were incubated at 37 °C in 1 mL phosphate-buffered saline solution (PBS, pH 7.4) containing the protease. The enzyme concentrations used in this test were 0.5 and 1.0 mg/mL [16]. The enzyme solution was replaced daily with freshly prepared solution. The control hydrogels were immersed in 1 mL PBS which was also refreshed daily. At designated time points (1, 3, 7 and 10 days), groups of samples were rinsed in distilled water and prepared for mass balance and scanning electron microscopy (SEM).

The percentage of weight loss [W (%)] of hydrogels was determined based on the following equation:

$$W\,(\%) = (W_0 - W_d)/W_0 \times 100$$

where W_0 is the initial weight of the hydrogel sample and W_d is the weight of the sample after degradation at predetermined days.

2.4. Biodegradation and bioactivity assessment in SBF

The *in vitro* degradation and bioactivity of the hydrogels were carried out using standard simulated body fluid (SBF) containing inorganic ion concentrations similar to those of human blood plasma [17]. The SBF solution was prepared by dissolving NaCl (8.035 g), $NaHCO_3$ (0.355 g), KCl (0.225 g), $K_2HPO_4.3H_2O$ (0.231 g), $MgCl_2.6H_2O$ (0.311 g), $CaCl_2$ (0.292 g) and Na_2SO_4 (0.072 g) into 700 mL ultrapure water. The solution was buffered at physiological pH 7.4 with Tris buffer (6.118 g) and HCl. Then the total volume of solution was filled up to 1000 mL with ultrapure water [17].

Hydrogels sections with 7 mm diameter and 5 mm thickness were carefully transferred to 48-well plates and were soaked in ultrapure water overnight to reach swelling equilibrium. The gels were removed from ultrapure water, excess liquid was blotted from the surface with filter paper, and the gel masses were determined. Then, the samples were immersed separately in 20 mL SBF in closed falcon tubes at 37 °C for 1, 3, 7, 14 and 21 days. After the different incubation time-points, the materials were removed from SBF solution, washed with ultrapure water and prepared for mass balance. Finally the hydrogels were freeze-dried, sectioned and viewed using SEM for apatite layer formation.

2.5. SEM

SEM was used to observe the morphology of samples after enzymatic degradation with protease XIV solution, as well as the apatite layer formation in the hydrogels after immersion in SBF. The analysis was performed on samples sputter coated (SPI-Module) with a thin gold/palladium film and then examined by SEM using a FEI Quanta 400 FEG/ESEM (FEI) scanning electron microscope at an accelerating voltage of 15 kV.

2.6. In vitro biological studies

2.6.1. hBMSCs isolation and culture

Human Bone Marrow Stromal Cells (hBMSCs) were obtained from bone marrow following orthopaedic surgery procedures, with patient's informed consent (male patients, 25–45 years old). The bone fragments (which would be otherwise discharged) were broken in small pieces and washed with alpha minimum essential medium (α-MEM, Sigma-Aldrich) supplemented with 10% (v/v) fetal bovine serum (FBS, Gibco), 100 IU/mL/2.5 μg/mL penicillin-streptomycin solution (Gibco) and 2.5 μg/mL amphotericin B (Gibco). The cell suspension was seeded in Petri dishes for 10 days. Afterwards, at 70–80% confluence, the cell monolayer was washed with PBS twice and cells were detached with trypsin solution (0.04%, Gibco) and subcultured. All assays were conducted with cells in passage 4.

Prior to cell seeding, the hydrogel sections with 7 mm diameter and 5 mm thickness were sterilized in ethanol solution at 70% (v/v) and subsequently washed twice with phosphate-buffered saline (PBS). For cell seeding, a suspension of 10^5 cells/scaffold was added on the top of each hydrogel. For the osteogenic medium, the above described medium was supplemented with 10 mM β-glycerophosphate (Sigma) and 10^{-8} M dexamethasone (Sigma). The seeded scaffolds were incubated in a humidified atmosphere of 95% air and 5% CO_2 at 37 °C. All samples were cultured for 1, 7, 14 and 21 days. The hBMSCs-seeded hydrogels were assessed for cell viability, proliferation, alkaline phosphatase (ALP) activity, total protein content, and F-actin cytoskeleton,

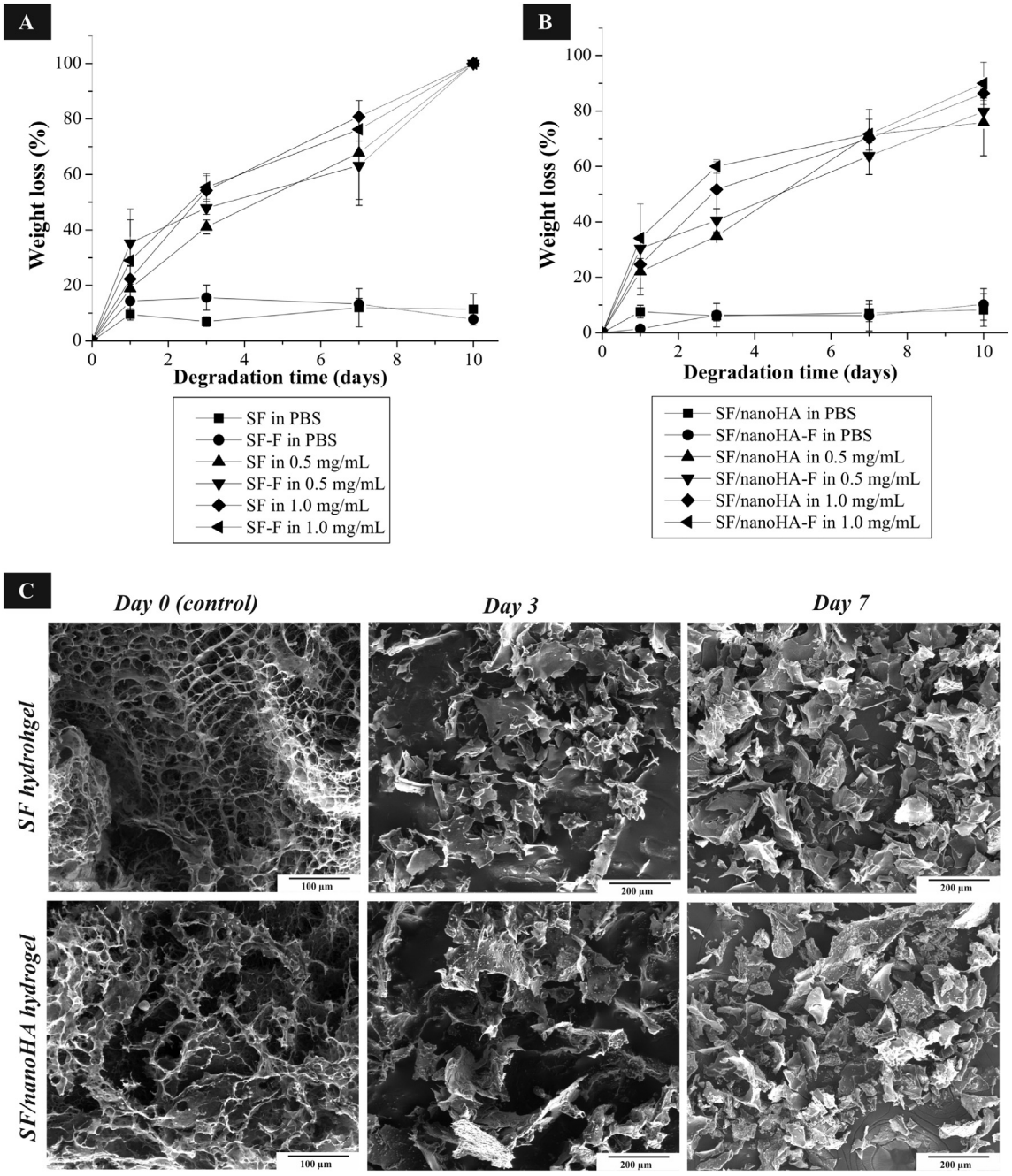

Fig. 1. Weight loss of non-frozen and frozen (A) SF and (B) SF/nanoHA hydrogels over time during a degradation period of 10 days by protease, and (C) SEM images of frozen hydrogels before degradation and after 3 and 7 days of degradation.

ALP and BMP-2 immunostaining. The SF hydrogels were used as controls of the SF/nanoHA hydrogels.

2.6.2. Metabolic activity

At each time point, the metabolic activity was evaluated by the resazurin assay. The same sample was followed throughout the culture time, *i.e.* it was assessed at all-time points. In the resazurin assay, a non-fluorescent blue component is reduced by the living cells to a pink fluorescent component. Fresh medium with 10% (v/v) of resazurin was added to the cells, which were incubated at 37 °C in a humidified atmosphere of 95% air and 5% CO_2 for 3 h. Then, 100 µL were transferred to a 96-well plate and the fluorescence intensity was measured in a microplate reader (Synergy HT, BioTek) at 535 nm excitation wavelength and 590 nm emission wavelength.

2.6.3. DNA content

Cell proliferation was assessed by the DNA extraction assay, at days 1, 7, 14 and 21. DNA content was measured using the PicoGreen DNA quantification assay (Quant-iT™ Picogreen dsDNA assay, Molecular Probes, Invitrogen), according to the manufacturer's instructions. After washing the hydrogels with PBS, they were immersed in 0.5 mL of ultrapure water and placed at 37 °C/5% CO_2 for 1 h, and then placed in a freezer at −80 °C. Subsequently, the hydrogels were thawed at room temperature to lyse the cell membranes. The fluorescence intensity was measured in a microplate reader (Synergy HT, BioTek) at 480 and 520 nm, excitation and emission, respectively.

2.6.4. Alkaline phosphatase activity and protein content

At each time point, colonized hydrogels were washed twice with

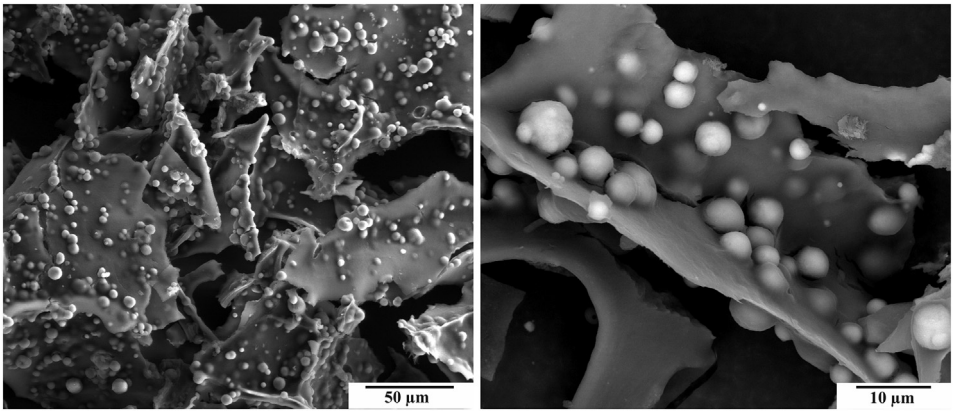

Fig. 2. NanoHA distribution in the SF/nanoHA hydrogels after the enzymatic degradation of the porous structure.

PBS and immersed in 0.5 mL ultrapure water at 37 °C/5% CO_2 for 1 h. They were then placed in a freezer at −80 °C and then thawed at room temperature to lyse the cell membranes. Alkaline phosphatase (ALP) activity was assayed by the hydrolysis of p-nitrophenol phosphate (Sigma), in alkaline buffer solution, 2-amino-2-methyl-1-propanol (Sigma), at pH 10.5. After 1 h of incubation at 37 °C, the reaction was stopped by adding NaOH (5 M, Sigma), and the absorbance of the hydrolysis product (p-nitrophenol) was measured at 405 nm, using a plate reader (BioTek). ALP activity was normalized to total protein content and was expressed as nanomoles of p-nitrophenol produced per minute per microgram of total protein (nmol min^{-1}/µg protein). Total protein content was measured by Lowry's method with bovine serum albumin used as a standard.

2.6.5. F-actin cytoskeleton, ALP and BMP-2 immunostaining

For F-actin cytoskeleton and BMP-2 immunostaining, seeded hydrogel samples were fixed in 3.7% formaldehyde (Sigma) for 15 min and washed twice with PBS. Then, cells were permeabilized with 0.1% (v/v) Triton X-100 solution (Sigma) for 30 min. Afterwards, samples were washed twice in PBS and incubated in 1% bovine serum albumin solution in PBS (BSA, Sigma) for 30 min to avoid nonspecific binding. For F-actin cytoskeleton immunostaining, cells were stained with Alexafluor phalloidin 488 (Invitrogen) in 1% BSA solution for 30 min at room temperature. Samples were washed twice with PBS and cell nuclei were stained with a buffer of Propidium iodide and RNase (BD Pharmigen) for 10 min. For BMP-2 immunostaining, cells were incubated with the primary antibody rabbit anti-BMP2 (1:200; Abcam) overnight at 4 °C. Samples were then washed twice in PBS and incubated with the secondary antibody Alexa Fluor 488 goat anti-rabbit igG for 1 h (1:1000; Molecular Probes).

ALP staining was performed in live cells by using an Alkaline Phosphatase (AP) Live Stain kit (Molecular Probes, Life Technologies), according to the manufacturer's instructions. Briefly, the culture medium was removed and the seeded hydrogels were washed twice with fresh medium. Then, and appropriate amount of 1X AP Live Stain solution was directly applied to the seeded hydrogels, followed by a 30 min incubation. Finally, the AP Live Stain was removed and the hydrogels were washed twice with fresh medium.

Immunostained hydrogels were observed under a Spectral Confocal Microscope Leica TCS-SP5 AOBS (Leica).

2.7. Statistical analysis

The results were expressed as the average ± standard deviation. There independent experiments were performed with culture established from different donors and each experiment was done in triplicate. The statistical analysis of the results was carried out using the one-way analysis of variance (ANOVA) followed by *post hoc* Tukey HSD multiple comparison test. Levels of $p < 0.05$ were considered to be statistically significant.

3. Results

3.1. Enzymatic degradation

The degradation behavior of the SF and SF/nanoHA hydrogels was assessed by incubating the materials in protease XIV and PBS (as a control) to evaluate quantitative changes. Fig. 1A and B show the weight loss of the SF and SF/nanoHA hydrogels, respectively, over time during a degradation period of 10 days. All materials presented progressive loss of mass by enzymatic hydrolysis over time. In contrast to SF hydrogels, which were fully degraded within 10 days, the percentage of weight loss of non-frozen and frozen SF/nanoHA hydrogels was 75.8% and 79.7%, respectively, for protease concentration of 0.5 mg/mL. Using the protease concentration of 1.0 mg/mL the degradation was 86.3% and 89.9% for non-frozen and frozen composite hydrogels, respectively. The differences between non-frozen and frozen hydrogels were not significant ($p > 0.05$) at any of the time points for both protease concentrations. The hydrogels incubated in PBS showed no significant degradation within 10 days and the structure integrity was maintained over time (data not shown).

Fig. 1C shows the morphological changes of hydrogels before degradation and after 3 and 7 days degradation by protease XIV. Similar morphological changes were observed for non-frozen and frozen hydrogels, and therefore only SEM images of frozen materials are shown. Before incubation, the porous structure of SF and SF/nanoHA hydrogels was intact and with interconnected pores (Fig. 1C). After incubation in the enzyme solution, the morphology of both hydrogels exhibited a drastic change, where the hydrogels could not keep its original form and collapsed, completely losing the porous structure.

Although a significant degradation was also observed in the composite hydrogels, an interesting phenomenon concerning to nanoHA distribution could not be neglected. As shown in Fig. 2, after the degradation of the porous structure it was clearly visible that the nanoHA aggregates were deposited uniformly in the SF matrix.

3.2. Apatite forming ability

3.2.1. Morphology and EDS analysis

The bioactive character of the hydrogels was tested *in vitro* by analyzing the ability to form apatite at their surface after being immersed in SBF. The prepared materials were immersed in SBF up to 21 days. Fig. 3 shows the SEM images of apatite layer formation on the hydrogels after 7 and 21 days. Similar apatite formation was observed for non-frozen and frozen hydrogels, and therefore only SEM images of frozen materials are shown. After 7 days in SBF, apatite structures had

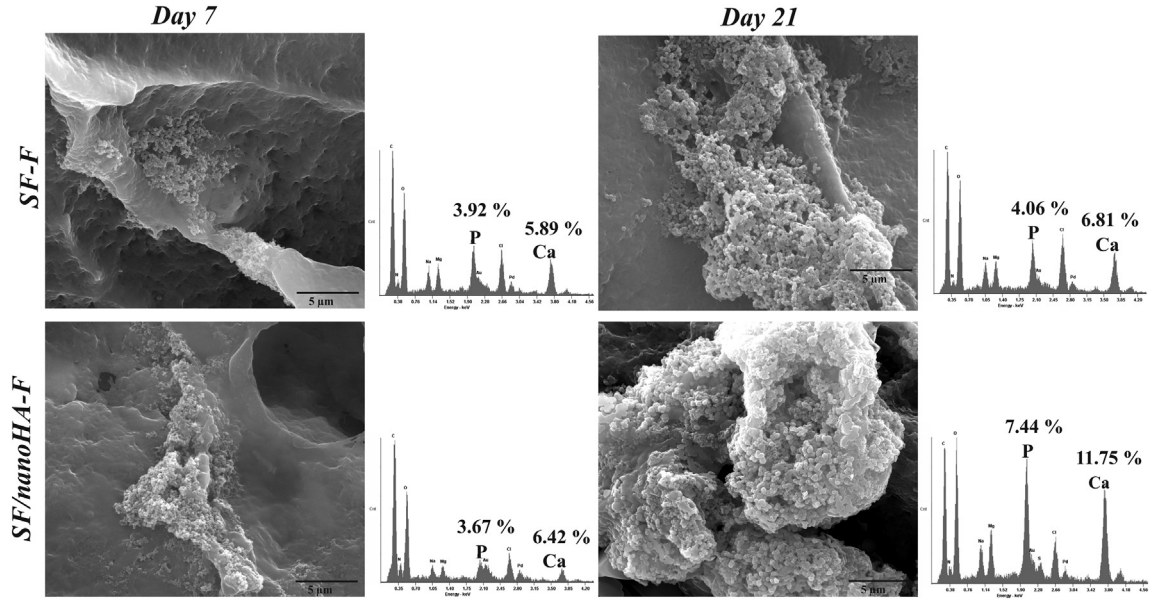

Fig. 3. SEM images and respective EDS spectra of frozen SF and SF/nanoHA hydrogels showing the formation of apatite after 7 and 21 days of immersion in SBF. The weight percentages of Ca and P are shown in the EDS spectra.

already been formed. After 21 days in solution, the apatite layer increased in density and was distributed over the entire surface of the two hydrogels. A more marked apatite formation was seen on hydrogels containing nanoHA.

The analysis of the energy dispersive spectroscopy (EDS) spectra of the frozen SF and SF/nanoHA hydrogels revealed the presence of the Ca and P elements, which corresponds to an apatite-like layer (Fig. 3). The weight percentages of Ca and P were similar for both hydrogels at day 7. Nevertheless, at day 21, the percentage of these elements only slightly increased for SF hydrogels while presenting a significant increase for SF/nanoHA hydrogels.

3.2.2. Degradation

Fig. 4 shows the weight loss of non-frozen and frozen SF and SF/nanoHA hydrogels in SBF at various time intervals. The mass of non-frozen and frozen SF hydrogels did not significantly change over 21 days. The weight loss of non-frozen and frozen composite hydrogels was also not significant until day 14. However, afterwards, the weight loss of these composites continuously decreases so that, at day 21, the samples gained weight when comparing to the initial value, before immersion in SBF, meaning that a deposit has been formed. This observation is in agreement with the results reported in the previous section, showing significant apatite formation in the composites, at later incubation times, compared to that observed in SF hydrogels.

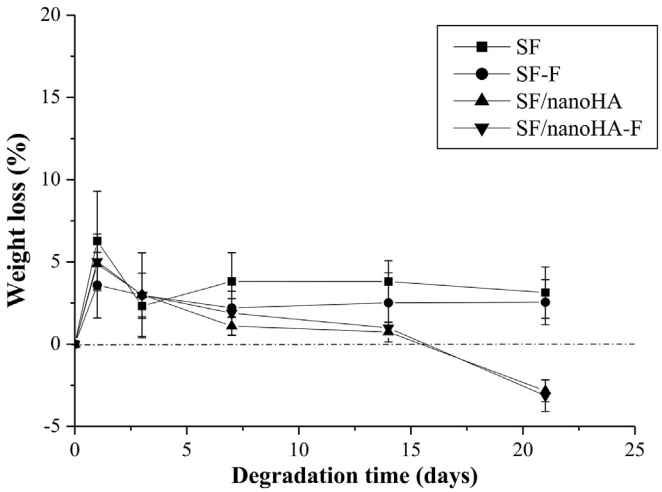

Fig. 4. Weight loss of non-frozen and frozen SF and SF/nanoHA hydrogels in SBF at various time intervals.

3.3. Biological studies

3.3.1. Cell metabolic activity and proliferation

Fig. 5 shows the results of the metabolic activity, DNA quantification and confocal microscopy images for the SF and SF/nanoHA hydrogels seeded with hBMSCs, at different time-points.

Metabolic activity increased throughout the 21 days culture time for all tested hydrogels. For non-frozen SF and SF/nanoHA hydrogels, no significant differences in metabolic activity were observed, except for a slightly increased value for the composite hydrogel at day 21. On the contrary, for frozen materials, a significant increase in metabolic activity was observed for SF/nanoHA hydrogels at day 14 (> 100%) and, particularly, at day 21 (~3 fold), comparatively to SF hydrogels. When comparing the materials of these two groups, non-frozen and frozen, no significant differences in metabolic activity were observed for SF hydrogels; however, the frozen SF/nanoHA hydrogels presented significantly increased values at days 14 and 21.

Concerning to DNA content, the same trend of cell response was observed for SF and SF/nanoHA hydrogels, considering non-frozen and frozen samples.

CLSM images of the frozen hydrogels showed that hBMSCs easily attached to the hydrogels and spread over the surface. At day 7, images showed cells with elongated morphology and cell-to-cell contact in both materials. At day 14, the cells were well spread out with notable cell-to-cell contact, forming an organized cell layer. At day 21, both hydrogels were completely covered with a dense cell layer. Images also suggested that the SF/nanoHA hydrogels showed a denser cell layer compared to SF hydrogels.

3.3.2. Alkaline phosphatase (ALP) activity and staining

ALP activity of hBMSCs cultured on non-frozen and frozen SF and SF/nanoHA hydrogels was analyzed at days 7, 14, and 21 (Fig. 6A). ALP activity on non-frozen SF/nanoHA and SF hydrogels was similar during the 21 days of culture. In contrast, in the frozen hydrogels, at day 21,

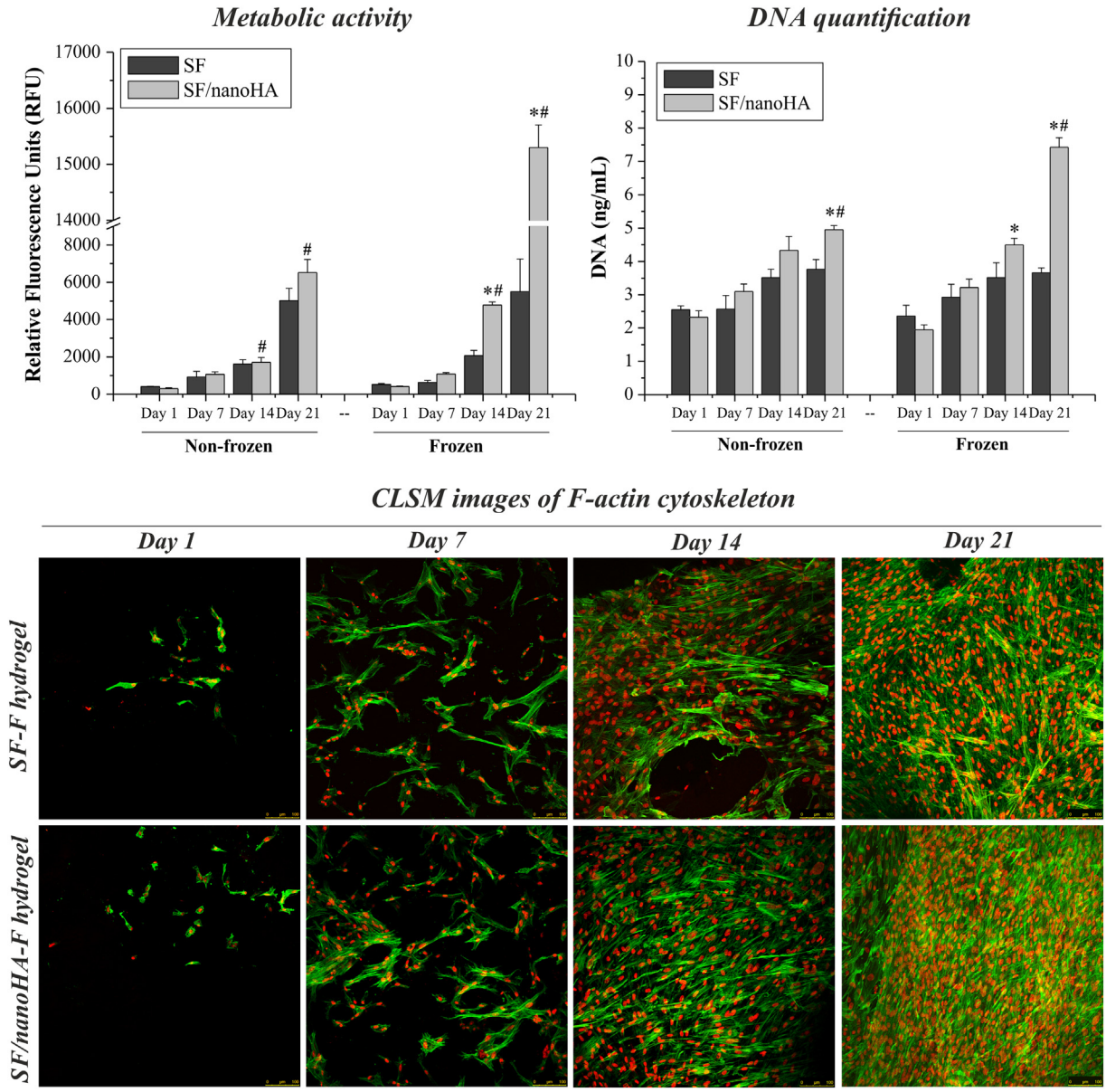

Fig. 5. Cell metabolic activity and DNA content of hBMSCs cultured on non-frozen and frozen SF and SF/nanoHA hydrogels, and CLSM images of hBMSCs on frozen SF and SF/nanoHA hydrogels, for 1, 7, 14 and 21 days of culture. * indicate significant differences ($p < 0.05$) between SF and SF/nanoHA hydrogels at the same culture time. # indicate significant differences ($p < 0.05$) between non-frozen and frozen SF/nanoHA hydrogels. Data are presented as the average ± SD. hBMSCs cells were stained for F-actin cytoskeleton with Alexafluor phalloidin (green) and nuclei with Propidium iodide (red). (For interpretation of the references to colour in this figure legend, the reader is referred to the web version of this article.)

ALP activity of SF/nanoHA hydrogels was significantly higher than that for SF hydrogels.

The presence of ALP was also examined in live cells, using an alkaline live stain (Fig. 6B). The ALP live stain showed that the cells were alive, functional, and homogeneously distributed throughout the hydrogels. On the SF hydrogel, stained cells were seen dispersed through the sample with irregular morphology and areas of higher intensity staining. Better cell response appears to occur with the SF/nanoHA composites. Cells presented elongated morphologies, with uniform ALP staining, cell-to-cell contact and establishing a continuous cell layer.

3.3.3. BMP-2 expression

The BMP-2 protein expression was investigated through immunostaining analysis as shown in Fig. 7. A strong staining intensity of BMP-2 expression was observed, at 21 days of culture, on frozen SF/nanoHA hydrogels in comparison to SF materials.

3.3.4. Cellular ingrowth inwards the porous structure

Fig. 8 presents a sequence of CLSM images showing a detail of the cell growth observed in the colonized frozen SF/nanoHA hydrogel inside a pore, at 21 days of culture. Clear evidence of cell infiltration through the pores was observed. Additionally, cells stained intensively for ALP through the porous structure, evidencing their functional activity both at the surface and within the pores walls.

4. Discussion

The incorporation of bioactive ceramics in biodegradable polymer matrices to produce three-dimensional (3D) scaffold materials is an additional design feature needed for bone tissue engineering applications. In a previous work, a SF hydrogel incorporating 15% (wt%) of nanoHA with larger pore sizes was developed. The micro- and macroporosity obtained combined with interconnective porous structure and

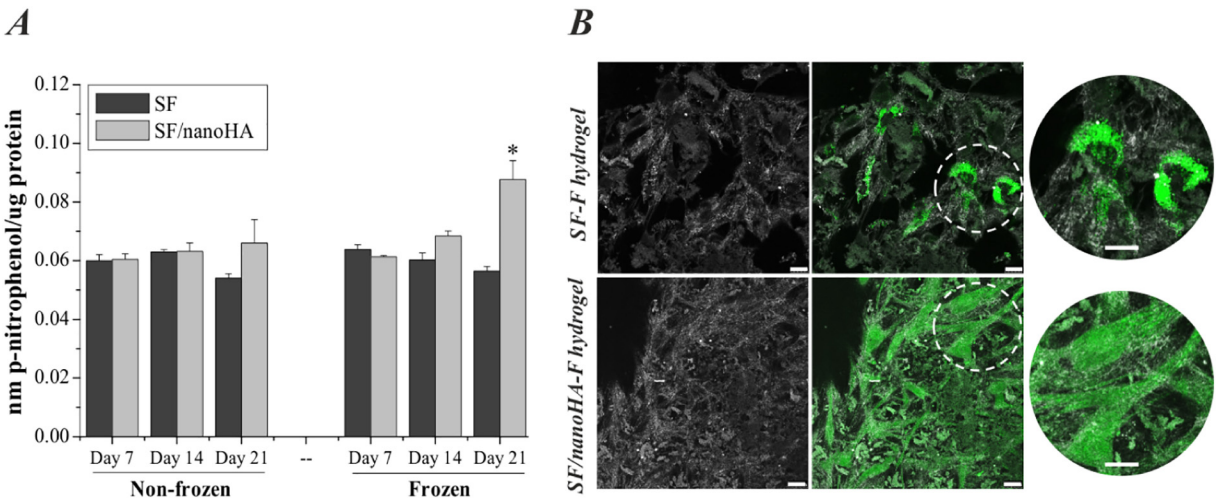

Fig. 6. (A) ALP activity of hBMSCs on non-frozen and frozen SF and SF/nanoHA hydrogels for 7, 14 and 21 days of culture, and (B) fluorescence images showing hBMSCs stained for ALP on frozen SF and SF/nanoHA hydrogels at 21 days. * indicate significant differences ($p < 0.05$) in relation to SF hydrogel at the same culture time. Data are presented as the average ± SD. Scale bar: 25 μm.

a uniform dispersion of nanoHA particles throughout the fibroin matrix, makes this composite hydrogel a very promising alternative to be applied in bone regeneration. Therefore, the main goal of this work was to exploit the *in vitro* biological response of this SF/nano hydrogel using human bone marrow stromal cells.

An appropriate degradation rate of the hydrogels is essential for bone tissue regeneration. It is desired that the scaffold degradation rate *in vivo* might match the rate of *de novo* tissue formation so that the porous structure is replaced by new tissue [18]. *In vitro* enzymatic hydrolysis provides a general idea of the biodegradability of a material. Generally, the enzymatic degradation of biomaterials is a two-step process. At first, proteolytic enzymes are adsorbed to the SF biomaterials, which demands that the enzymes must find binding domains on the material's surface. Afterwards, SF biomaterials are enzymatically digested leading to the corresponding amino acids, which are easily disposed *in vivo*, an advantage of SF used in the biomedical applications [19,20]. In the present work, while the SF hydrogels incubated with the protease were fully degraded within 10 days, the materials incubated in phosphate buffer showed no significant degradation, confirming that the mass loss was due solely to enzymatic hydrolysis. This marked degradation shows the potential of SF as a biodegradable material. Additionally, with the incorporation of nanoHA aggregates into the hydrogels the degradation rate was similar to that found in control SF materials. Furthermore, a uniform dispersion of nanoHA particles throughout the fibroin matrix was observed after the enzymatic degradation, which is crucial for a good performance of the composite hydrogel in bone tissue engineering. The degradation rate and the morphological structure changes were similar for the non-frozen and frozen hydrogels, suggesting that pore size did not correlate to degradation rate. This is in agreement with previous results reported by Kim U. et al. in SF scaffolds with different pore sizes exposed to a protease solution [21].

To be effectively used for bone tissue regeneration, it is beneficial that a material might promote bone-like apatite formation when in

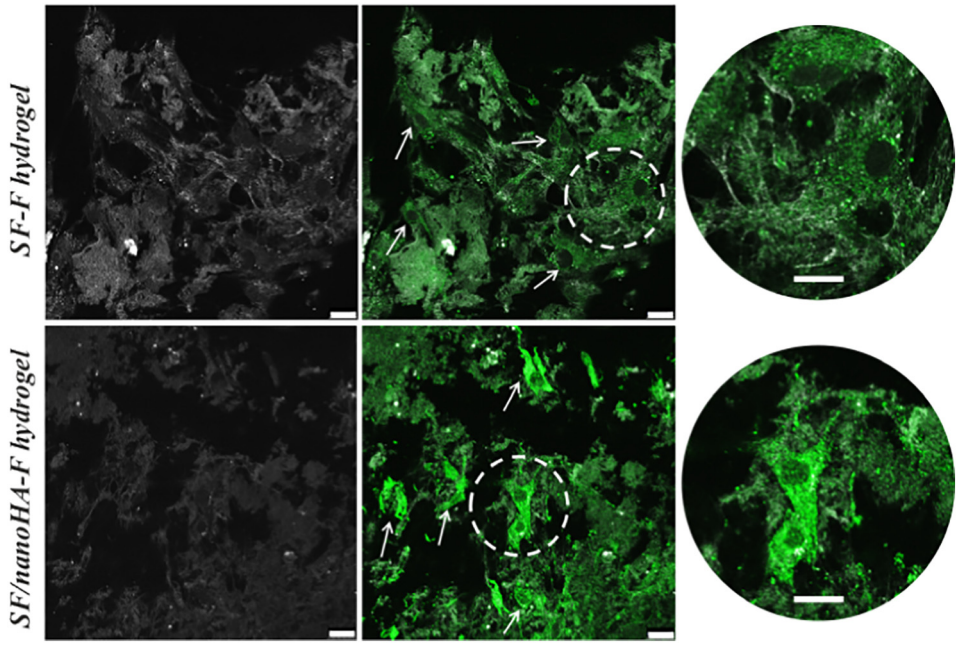

Fig. 7. Fluorescence images showing the frozen SF and SF/nanoHA hydrogels and the BMP-2 expression in hBMSCs cultured on frozen SF and SF/nanoHA materials, indicated by the arrows, at 21 days. The zoomed images showed in more detail the BMP-2 expression in cells. Scale bar: 25 μm.

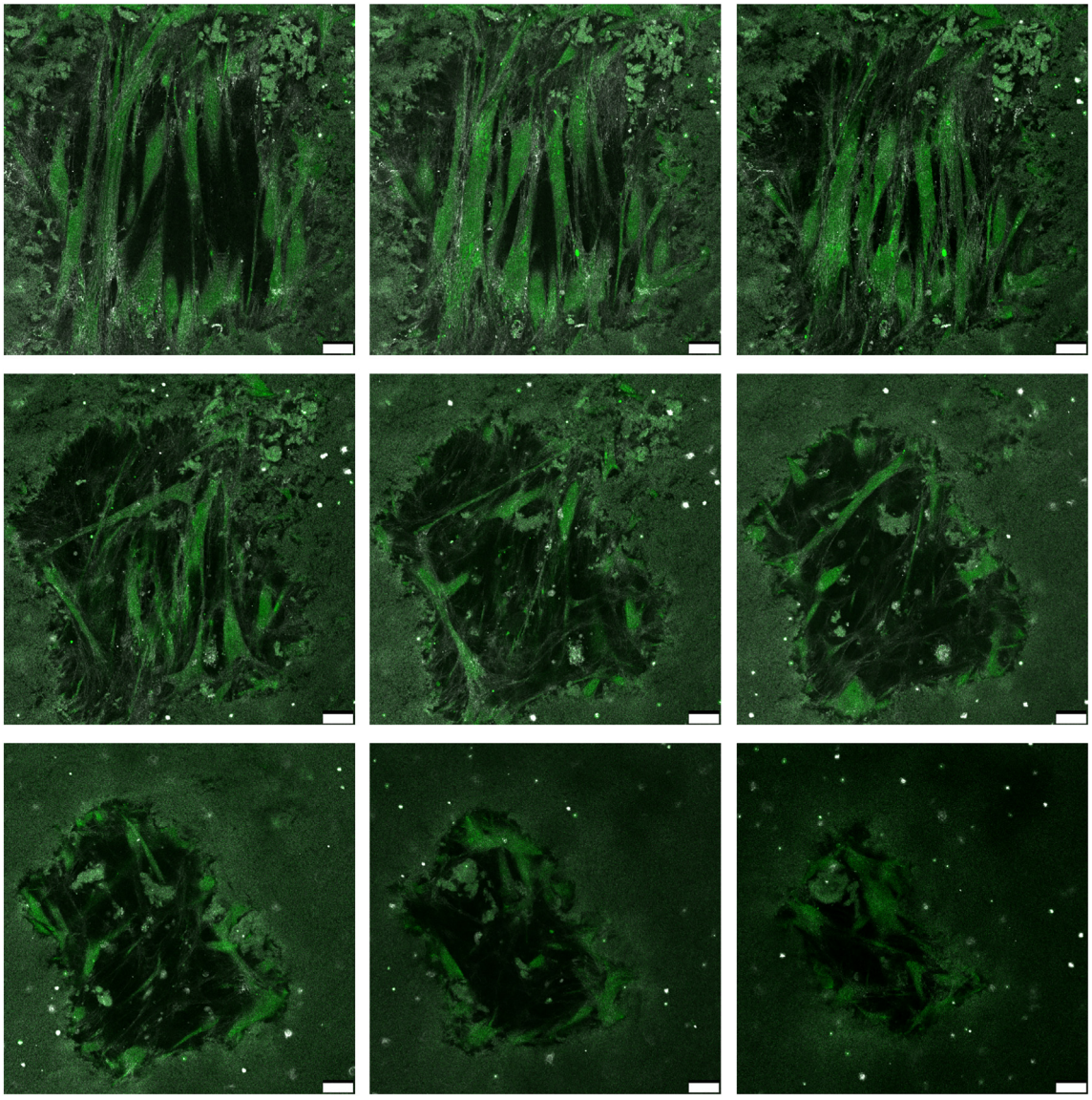

Fig. 8. Representative sequence of CLSM images showing the infiltration of hBMSCs on frozen SF/nanoHA composite hydrogel inside a pore, at 21 days of culture. Cells were stained with an ALP live stain (green). Scale bar: 25 μm. (For interpretation of the references to colour in this figure legend, the reader is referred to the web version of this article.)

contact with physiological fluid. SF and SF/nanoHA hydrogels were evaluated for their bioactivity using SBF. The morphological analysis combined with the EDS analysis confirmed the presence of a CaP layer on the surface of non-frozen and frozen SF and SF/nanoHA hydrogels. Nevertheless, the composite hydrogel containing nanoHA had greater ability to induce the apatite layer formation *in vitro*. The nanoHA aggregates in the composite could act as nucleation sites and consequently the apatite could be formed more effectively on the composite hydrogels than on the SF hydrogels. This is in line with previous studies performed in chitosan-gelatin scaffolds incorporating nanophase hydroxyapatite [22], also in a poly(L-lactic acid) (PLLA) matrix with the addition of HA particles [23]. Additionally, in the later study, the implantation of the apatite-coated poly(L-lactic acid)/hydroxyapatite (PLLA/HA) composite scaffold in the subchondral bone of healthy sheep femoral condyle yielded better integration in comparison to non-coated PLLA scaffolds [23]. Back to the present work, immersion of SF hydrogels in SBF did not result in significant weight loss during the 21 days. However, in the SF/nanoHA hydrogels, the weight increased from day 14 until day 21, which could be attributed to deposition of apatite particles (Ca^{2+} and PO_4^{3-} ions) on the surface of the composite hydrogels. The present results showed an improvement of bioactivity on the composite hydrogels indicating that these materials have great potential for bone tissue engineering.

Hydrogels for bone regeneration must be cytocompatible and actively encourage ingrowth of cells. As evaluated by the resazurin assay and DNA quantification, the increase of metabolic activity and proliferation, respectively, of hBMSCs on hydrogels over time indicated the cytocompatible of these materials. These results correlated well with confocal images that showed extensive cell spreading and proliferation within the hydrogels. For later culture times, the hBMSCs cultured in the hydrogels with nanoHA proliferated significantly, showing an inductive effect of the presence of nanoHA. Previous studies had also proven that the inclusion of nanoHA in scaffolds of pullulan and dextran could enhance the proliferation of hBMSCs in the hydrogels [24]. Moreover, this tendency was particularly confirmed in the case of frozen SF/nanoHA hydrogels, showing that the increase of pore size of frozen materials [8] may play a prominent role in metabolic cell activities and proliferation. Bhardwaj N et al. also reported that the metabolic activity and proliferation ability of the cells was higher in SF/chitosan scaffolds with larger pores [25].

One of the most attractive characters that hBMSCs show is their multiple differentiation potential. Under appropriate conditions, hBMSCs are able to differentiate towards several cell lineages, including osteoblasts, adipocytes chondrocytes, and myocytes. Differentiation is induced through addition of "cocktails" of morphogens and chemicals inducing the differentiation of a particular cell type. *In vitro,* differentiation is verified by demonstrating the induction of specific gene expression and proteins [26–28]. In osteogenesis, differentiation of hBMSCs into osteoblasts is a key step and ALP is an important early marker for cells undergoing differentiation to form osteoblast [29]. ALP activity, normalized as a function of the protein content, was the highest in the case of frozen SF/nanoHA composite hydrogels at 21 days of culture, showing the efficacy of nanoHA aggregates in enhancing the osteoblastic phenotype expression level. Furthermore, it is worth noting that this difference in ALP expression between frozen SF and SF/nanoHA materials was observed in a quantitative assay and also in a live cell staining. Several other works can be found in the literature indicating the effect of nanoHA in the ALP expression in different composite materials, such as poly(L/DL)-lactide/nanoHA membranes [30], nanoHA/polyamide scaffolds [31], and poly(L-lactic acid)/poly-benzyl-L-glutamate/collagen/nanoHA scaffolds [32].

Immunofluorescent staining of BMP-2 protein showed greater expression in the SF/nanoHA composite hydrogels compared to that of control SF materials. Bone morphogenetic proteins (BMPs) play an important role in osteoblast differentiation and deposition of bone matrix. The high osteoinductive potential of some BMPs is illustrated by their ability to induce bone formation. Among them, BMP-2 protein is essential to induce the expression of Runt-related transcription factor 2 (Runx-2) and Osterix, the two critical transcription factors in osteoblast differentiation. Runx-2 is the main regulator for the expression of downstream key genes, as collagen type I, alkaline phosphatase, osteopontin, bone sialoprotein and osteocalcin, at an early stage of osteoblastic differentiation. Runx-2 has also a role in the regulation of the Osterix expression, a later key transcription factor for osteoblastic differentiation, which is involved in collagen type I and osteocalcin gene activation, being also a downstream regulator for Runx-2 activity [33–36].

Hydrogels should have the ability to regenerate functional bone tissue at the site of injury through a cell migration process in a carefully orchestrated manner. Initial attachment of cells is especially critical for long-term cells stability and differentiation. The ability of the composite hydrogel to support hBMSCs adhesion and proliferation was also evaluated using a live cell fluorescence staining for ALP. CLSM images showed that hBMSCs were able to infiltrate and migrate within the hydrogel, through the porous structure. We strongly believe that cell infiltration occurs towards inside the pores – images clearly show that the cell density is higher on the surface (top of the pore) and progressively decreases towards inside the pore. We believe that if the cells were deposited inside the pore in the first place (during the cell seeding procedure), formation of organized cell groupments would be visible inside the pores as a result of the cell proliferation throughout the 21-day culture time. Images show progressively decreased cell numbers towards inside the pore, suggesting a progressive cell infiltration process. Furthermore, one interesting finding in this work was that ALP expression in hBMSCs was observed within the SF/nanoHA hydrogel, indicating not only cell infiltration into the material, but also active production of ALP by the infiltrated cells.

The results of the current work support the potential of this composite hydrogel as a material for stimulating new bone tissue formation.

5. Conclusions

Advances in bone tissue engineering require biofunctional hydrogels that interact with bone forming cells. To achieve this goal, a SF/nanoHA composite hydrogel with improved bioactivity was developed. The SF/nanoHA hydrogels can act as matrix for hBMSCs viability and proliferation, which was significantly improved on frozen composite materials. Confocal images showed that hBMSCs could spread and proliferate on these hydrogels during 21 days of culture. Furthermore, an improvement of the osteogenic response, as seen by ALP and BMP-2 expression, was observed for composite materials. Also, evident infiltration of functionally active cells through the porous hydrogel structure was noticed.

Acknowledgements

This work was financed by FEDER - Fundo Europeu de Desenvolvimento Regional funds through the COMPETE 2020 – Operacional Programme for Competitiveness and Internationalisation (POCI), Portugal 2020, and by Portuguese funds through FCT - Fundação para a Ciência e a Tecnologia/Ministério da Ciência, Tecnologia e Inovação in the framework of the project "Institute for Research and Innovation in Health Sciences (POCI-01-0145-FEDER-007274)" and PhD grant (SFRH/BD/90400/2012), whose support is acknowledged. Financial support from the European Union (FEDER funds POCI/01/0145/FEDER/007265) and National Funds (FCT/MEC, Fundação para a Ciência e Tecnologia and Ministério da Educação e Ciência) under the Partnership Agreement PT2020 UID/QUI/50006/2013, is also acknowledged. The authors thank FLUIDINOVA S.A. (Maia-Portugal) for the provision of nanoHA.

References

[1] F. Tortelli, R. Cancedda, Three-dimensional cultures of osteogenic and chondrogenic cells: a tissue engineering approach to mimic bone and cartilage in vitro, Eur. Cell. Mater. 17 (2009) 1–14.
[2] D.W. Hutmacher, J.T. Schantz, C.X. Lam, K.C. Tan, T.C. Lim, State of the art and future directions of scaffold-based bone engineering from a biomaterials perspective, J. Tissue Eng. Regen. Med. 1 (2007) 245–260.
[3] H.S. Azevedo, F.M. Gama, R.L. Reis, In vitro assessment of the enzymatic degradation of several starch based biomaterials, Biomacromolecules 4 (2003) 1703–1712.
[4] A.H. Annor, M.E. Tang, C.L. Pui, G.C. Ebersole, M.M. Frisella, B.D. Matthews, C.R. Deeken, Effect of enzymatic degradation on the mechanical properties of biological scaffold materials, Surg. Endosc. 26 (2012) 2767–2778.
[5] M. Ahearne, Y. Yang, A.J. El Haj, K.Y. Then, K.K. Liu, Characterizing the viscoelastic properties of thin hydrogel-based constructs for tissue engineering applications, J. R. Soc. Interface 2 (2005) 455–463.
[6] N.A. Peppas, J.Z. Hilt, A. Khademhosseini, R. Langer, Hydrogels in biology and medicine: from molecular principles to bionanotechnology, Adv. Mater. 18 (2006) 1345–1360.
[7] H. Geckil, F. Xu, X. Zhang, S. Moon, U. Demirci, Engineering hydrogels as extracellular matrix mimics, Nanomedicine (Lond.) 5 (2010) 469–484.
[8] M. Ribeiro, M.A. de Moraes, M.M. Beppu, M.P. Garcia, M.H. Fernandes, F.J. Monteiro, M.P. Ferraz, Development of silk fibroin/nanohydroxyapatite composite hydrogels for bone tissue engineering, Eur. Polym. J. 67 (2015) 66–77.
[9] D.N. Rockwood, R.C. Preda, T. Yucel, X. Wang, M.L. Lovett, D.L. Kaplan, Materials fabrication from *Bombyx mori* silk fibroin, Nat. Protoc. 6 (2011) 1612–1631.
[10] N. Bhardwaj, S. Chakraborty, S.C. Kundu, Freeze-gelled silk fibroin protein scaffolds for potential applications in soft tissue engineering, Int. J. Biol. Macromol. 49 (2011) 260–267.
[11] A.J. Meinel, K.E. Kubow, E. Klotzsch, M. Garcia-Fuentes, M.L. Smith, V. Vogel, H.P. Merkle, L. Meinel, Optimization strategies for electrospun silk fibroin tissue engineering scaffolds, Biomaterials 30 (2009) 3058–3067.
[12] X. Hu, Q. Lu, L. Sun, P. Cebe, X. Wang, X. Zhang, D.L. Kaplan, Biomaterials from ultrasonication-induced silk fibroin–hyaluronic acid hydrogels, Biomacromolecules 11 (2010) 3178–3188.
[13] Q. Lv, K. Hu, Q. Feng, F. Cui, Fibroin/collagen hybrid hydrogels with crosslinking method: preparation, properties, and cytocompatibility, J. Biomed. Mater. Res. A 84 (2008) 198–207.
[14] D. Puppi, F. Chiellini, A.M. Piras, E. Chiellini, Polymeric materials for bone and cartilage repair, Prog. Polym. Sci. 35 (2010) 403–440.
[15] S.A. Poursamar, M. Azami, M. Mozafari, Controllable synthesis and characterization of porous polyvinyl alcohol/hydroxyapatite nanocomposite scaffolds via an in situ colloidal technique, Colloids Surf. B: Biointerfaces 84 (2011) 310–316.
[16] R. Rajkhowa, E.S. Gil, J. Kluge, K. Numata, L. Wang, X. Wang, D.L. Kaplan, Reinforcing silk scaffolds with silk particles, Macromol. Biosci. 10 (2010) 599–611.
[17] T. Kokubo, H. Takadama, How useful is SBF in predicting in vivo bone bioactivity? Biomaterials 27 (2006) 2907–2915.
[18] L. Nie, D. Chen, J. Fu, S. Yang, R. Hou, J. Suo, Macroporous biphasic calcium phosphate scaffolds reinforced by poly-L-lactic acid/hydroxyapatite nanocomposite coatings for bone regeneration, Biochem. Eng. J. 98 (2015) 29–37.
[19] L.S. Nair, C.T. Laurencin, Biodegradable polymers as biomaterials, Prog. Polym. Sci.

32 (2007) 762–798.
[20] Y. Cao, B. Wang, Biodegradation of silk biomaterials, Int. J. Mol. Sci. 10 (2009) 1514–1524.
[21] U.J. Kim, J. Park, H.J. Kim, M. Wada, D.L. Kaplan, Three-dimensional aqueous-derived biomaterial scaffolds from silk fibroin, Biomaterials 26 (2005) 2775–2785.
[22] M. Peter, N. Ganesh, N. Selvamurugan, S.V. Nair, T. Furuike, H. Tamura, R. Jayakumar, Preparation and characterization of chitosan–gelatin/nanohydroxyapatite composite scaffolds for tissue engineering applications, Carbohydr. Polym. 80 (2010) 687–694.
[23] H. Deplaine, M. Lebourg, P. Ripalda, A. Vidaurre, P. Sanz-Ramos, G. Mora, F. Prosper, I. Ochoa, M. Doblare, J.L. Gomez Ribelles, I. Izal-Azcarate, G. Gallego Ferrer, Biomimetic hydroxyapatite coating on pore walls improves osteointegration of poly(L-lactic acid) scaffolds, J Biomed Mater Res B Appl Biomater 101 (2013) 173–186.
[24] J.C. Fricain, S. Schlaubitz, C. Le Visage, I. Arnault, S.M. Derkaoui, R. Siadous, S. Catros, C. Lalande, R. Bareille, M. Renard, T. Fabre, S. Cornet, M. Durand, A. Leonard, N. Sahraoui, D. Letourneur, J. Amedee, A nano-hydroxyapatite—pullulan/dextran polysaccharide composite macroporous material for bone tissue engineering, Biomaterials 34 (2013) 2947–2959.
[25] N. Bhardwaj, S.C. Kundu, Chondrogenic differentiation of rat MSCs on porous scaffolds of silk fibroin/chitosan blends, Biomaterials 33 (2012) 2848–2857.
[26] M. Kassem, B.M. Abdallah, H. Saeed, Osteoblastic cells: differentiation and trans-differentiation, Arch. Biochem. Biophys. 473 (2008) 183–187.
[27] J. Rauh, F. Milan, K.P. Gunther, M. Stiehler, Bioreactor systems for bone tissue engineering, Tissue Eng. Part B Rev. 17 (2011) 263–280.
[28] H. Lu, L. Lian, D. Shi, H. Zhao, Y. Dai, Hepcidin promotes osteogenic differentiation through the bone morphogenetic protein 2/small mothers against decapentaplegic and mitogen-activated protein kinase/P38 signaling pathways in mesenchymal stem cells, Mol. Med. Rep. 11 (2015) 143–150.
[29] G.A. Fielding, M. Roy, A. Bandyopadhyay, S. Bose, Antibacterial and biological characteristics of silver containing and strontium doped plasma sprayed hydroxyapatite coatings, Acta Biomater. 8 (2012) 3144–3152.
[30] I. Rajzer, E. Menaszek, R. Kwiatkowski, W. Chrzanowski, Bioactive nanocomposite PLDL/nano-hydroxyapatite electrospun membranes for bone tissue engineering, J. Mater. Sci. Mater. Med. 25 (2014) 1239–1247.
[31] H. Wang, Y. Li, Y. Zuo, J. Li, S. Ma, L. Cheng, Biocompatibility and osteogenesis of biomimetic nano-hydroxyapatite/polyamide composite scaffolds for bone tissue engineering, Biomaterials 28 (2007) 3338–3348.
[32] R. Ravichandran, J.R. Venugopal, S. Sundarrajan, S. Mukherjee, S. Ramakrishna, Precipitation of nanohydroxyapatite on PLLA/PBLG/collagen nanofibrous structures for the differentiation of adipose derived stem cells to osteogenic lineage, Biomaterials 33 (2012) 846–855.
[33] Q. Kang, M.H. Sun, H. Cheng, Y. Peng, A.G. Montag, A.T. Deyrup, W. Jiang, H.H. Luu, J. Luo, J.P. Szatkowski, P. Vanichakarn, J.Y. Park, Y. Li, R.C. Haydon, T.C. He, Characterization of the distinct orthotopic bone-forming activity of 14 BMPs using recombinant adenovirus-mediated gene delivery, Gene Ther. 11 (2004) 1312–1320.
[34] H.K. Datta, W.F. Ng, J.A. Walker, S.P. Tuck, S.S. Varanasi, The cell biology of bone metabolism, J. Clin. Pathol. 61 (2008) 577–587.
[35] M. Raida, A.C. Heymann, C. Gunther, D. Niederwieser, Role of bone morphogenetic protein 2 in the crosstalk between endothelial progenitor cells and mesenchymal stem cells, Int. J. Mol. Med. 18 (2006) 735–739.
[36] M.H. Fernandes, P.S. Gomes, Bone cells dynamics during peri-implantitis: a theoretical analysis, J. Oral Maxillofac. Res. 7 (2016) e6.